Rapid Lightoff of Syngas Production from Methane: A Transient Product Analysis

Kenneth A. Williams, Corey A. Leclerc, and Lanny D. Schmidt
Dept. of Chemical Engineering and Materials Science, University of Minnesota, Minneapolis, MN 55455-0132

DOI 10.1002/aic.10294
Published online in Wiley InterScience (www.interscience.wiley.com).

Steady-state production of syngas (CO and H_2) can be attained within 10 s from room-temperature mixtures of methane and air fed to a short-contact-time reactor by initially operating at combustion stoichiometry ($CH_4/O_2 = 0.5$) and then quickly switching to syngas stoichiometry ($CH_4/O_2 = 2.0$). The methane/air mixture is first ignited, forming a premixed flame upstream of the catalyst that heats the Rh-impregnated α-alumina foam monolith to catalytic lightoff ($T > 500°C$) in a few seconds. The methane/oxygen ratio is then increased to partial oxidation stoichiometry, which extinguishes the flame and effects immediate autothermal syngas production. Transient species profiles are measured with a rapid-response mass spectrometer (response time constant ≅ 0.5 s), and catalyst temperature is measured with a thermocouple at the catalyst back face. Because the monolith thermal response time (~ 1 s) is several orders of magnitude larger than the reaction timescales (~ 10^{-12} to 10^{-3} s), chemistry and flow should be mathematically decoupled from local transient variations in catalyst temperature. Using this assumption, a transient temperature profile is combined with detailed surface chemistry for methane on Rh in a numerical plug-flow model. This approach accurately reproduces the transient species profiles measured during experimental lightoff for short combustion time experiments and lends insight into how the monolith temperature develops with time. The combined experimental and numerical efforts supply useful information on the transient reactor behavior for various combustion times and identify a combustion time to avoid undershoot or overshoot in catalyst temperature and minimize start-up time. *AIChE J,* 51: 247–260, 2005
Keywords: methane, catalytic partial oxidation, start-up, kinetic modeling, syngas

Introduction

Catalytic partial oxidation (CPO) of methane[1,2] and larger alkanes[3-5] to produce syngas at millisecond contact times offers a pathway to hydrogen production for small mobile power applications such as solid oxide and proton exchange membrane fuel cells. The global reaction for methane CPO is

$$CH_4 + 0.5O_2 \rightarrow CO + 2H_2 \qquad \Delta H_R^\circ = -35.6 \text{ kJ/mol } CH_4$$

and could be used instead of steam reforming:

$$CH_4 + H_2O \rightarrow CO + 3H_2 \qquad \Delta H_R^\circ = +206 \text{ kJ/mol } CH_4$$

The partial oxidation reaction is exothermic so it can operate autothermally. In contrast, steam reforming is endothermic, thus requiring a furnace that is difficult to scale down and slow to start up. A key benefit of a CPO reactor is that it can operate at gas hourly space velocities (GHSV) two to three orders of magnitude higher than a conventional steam reformer (10^5–10^6 h^{-1} vs. 10^3 h^{-1}) while giving similar yields, so it should be two

Present address of C. A. Leclerc: Dept. of Chemical Engineering, McGill University, Montreal, Quebec H3A 2B2, Canada.
Correspondence concerning this article should be addressed to L. D. Schmidt at schmi001@umn.edu.

to three orders of magnitude smaller than a steam reformer for the same production rate.

The relatively small footprint of CPO is attractive for applications that cannot accommodate a large fuel reformer, such as fuel cells to power automobiles or pollution abatement equipment for existing automotive engines. The positive impacts of hydrogen addition to the spark ignition engine on pollution abatement, especially during start-up, have motivated further research on both the onboard generation of hydrogen and the logistics of hydrogen delivery to the engine.[6,7] Rapid start-up of these compact systems will be crucial. Given the frequent start-ups and process fluctuations automotive reforming systems will face, they will be required to produce hydrogen from room-temperature mixtures in seconds and respond almost instantaneously to dramatic shifts in required power output. Therefore, the design and optimization of a compact reforming system capable of producing hydrogen within several seconds is a critical step toward creating enabling technologies that can rapidly generate energy with lower harmful emissions than current practices.

Studies on lightoff of methane CPO have yielded a range of start-up times. Use of an electrically heated Pd-coated metallic monolith gave a lightoff time of about 90 s.[8] A Rh-coated honeycomb monolith, preheated to 700 K with a furnace, gave a start-up time of about 120 s after ignition.[9] In comparison, it was shown that CPO on Rh-coated alumina foams produced hydrogen from methane in about 10 s without feed preheat in a fast lightoff reactor that initially made use of the combustion reaction[10]

$$CH_4 + 2O_2 \rightarrow CO_2 + 2H_2O \qquad \Delta H_R^\circ = -802 \text{ kJ/mol } CH_4$$

by igniting a stoichiometric mixture of methane and air ($CH_4/O_2 = 0.5$). The resulting premixed flame heated the catalyst to lightoff temperature (>500°C), after which the fuel-to-air ratio was increased to partial oxidation stoichiometry ($CH_4/O_2 = 2.0$) to extinguish the flame and allow autothermal syngas production. The time needed to reach steady-state syngas production was determined by the catalyst back-face temperature and analysis of samples obtained from the reactor effluent by gas chromatography.

The focus of the present study is the transient behavior of the catalyst foam during lightoff. In this work, the fast lightoff reactor is coupled with a fast-response mass spectrometer and data-acquisition system to quantify selectivities and methane conversion during the rapid start-up period. Additionally, numerical plug-flow models incorporating multistep surface chemistry are used to simulate the transient species profiles and investigate how the monolith temperature develops with time. The combined experimental and numerical efforts supply useful information on the transient reactor behavior for various combustion times and identify a combustion time to avoid undershoot or overshoot in catalyst temperature and minimize start-up time.

Materials and Methods

Experimental apparatus and procedure

High-purity reactant gases (CH_4, O_2, and Ar) were fed through calibrated mass flow controllers to regulate flow rates.

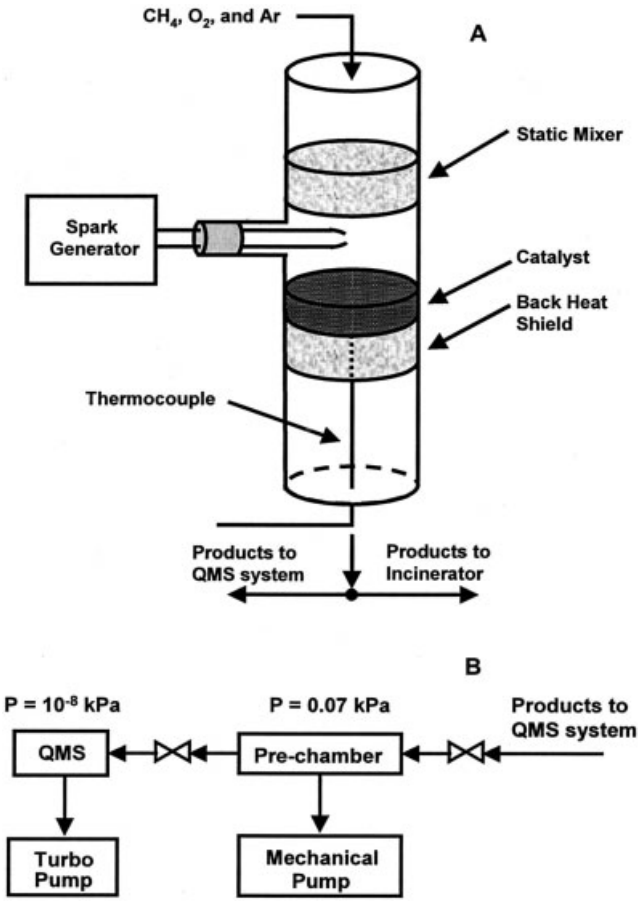

Figure 1. Fast lightoff reactor and quadrupole mass spectrometer (QMS) system schematics.

(A) A spark ignites the combustion feed, forming a flame above the catalyst. The resulting premixed flame heats the catalyst for a predetermined time (1–20 s), after which the fuel flow rate is increased to partial oxidation stoichiometry. During partial oxidation, carbon monoxide and hydrogen are made exclusively by surface chemistry. (B) Products are measured with a differentially pumped QMS system in which the products pass from the reactor outlet at 102 kPa to a pre-chamber at 0.07 kPa to the QMS at 10^{-8} kPa.

Premixed gases were fed through 0.64-cm inside diameter (ID) stainless steel tubing to the top of the reactor through a quartz endcap with a 0.64-cm ID side port.

The reactor consisted of a quartz tube approximately 19 mm ID × 40 cm long (Figure 1A). Reactants passed through a blank ceramic monolith, which acted as a mixer and flame holder during the lightoff combustion phase, and entered the ignition compartment where electrodes of a spark generator were placed immediately upstream from the catalyst. The catalyst, mixer, and back heat shield (behind the catalyst to attenuate axial heat losses) were 80 pores per linear inch (ppi) α-alumina foam monoliths. The catalytic monolith was 5 mm long × 18 mm diameter, whereas the mixer and back heat shield were 10 mm long × 18 mm diameter. All three monoliths were wrapped in alumino-silicate paper to make a tight seal before being placed inside the quartz tube. Foam monoliths were coated with γ-alumina washcoat to increase effective surface area and then coated with $Rh(NO_3)_3$ solution to give final Rh loadings of about 5% by weight. The rest of the

catalyst preparation was described previously.[11] The reactor temperature was measured at the catalyst back face with a 0.25-mm-diameter type K thermocouple (<0.3-s response time constant). The catalyst section was wrapped with ceramic blanket insulation to attenuate radial heat losses. Effluent gases flowed out of the reactor into heated stainless steel tubing.

The outlet flow was split after the bottom reactor endcap so that the majority of the flow was directed to an incinerator, whereas the remainder traveled to a differentially pumped quadrupole mass spectrometer (QMS) system for analysis. The gases for analysis entered a pre-chamber maintained at 0.07 kPa by a mechanical vacuum pump, passed into another chamber pumped down to 10^{-8} kPa by a turbomolecular pump, and then entered the QMS for mass separation and detection (Figure 1B).

The QMS system scanned masses 1 through 50 at about 3 Hz. Argon instead of nitrogen was used as the calibration diluent because nitrogen overlapped with carbon monoxide at mass 28. QMS signals for water (mass 18) are not reported because of water condensation in the system. The QMS signals were corrected using calibration curves that plotted the ratio of each component response over argon response vs. the ratio of each species actual concentration over argon concentration. Accurate product concentrations for various reactant ratios were determined through daily analysis with a gas chromatograph equipped with a thermal conductivity detector. Carbon and hydrogen atom balances typically closed to within 5% error.

Experimental control and data acquisition were automated using a computer workstation running LabVIEW® that allowed implementation of quick changes in reactant stoichiometry, control of the spark generator, combustion time input, and all experimental data to be written to a data file for analysis. Simulated air flow rates (79% Ar/21% O_2, or hereafter "air") were 5 to 9 standard liters per minute (slpm), whereas methane flow rates were adjusted accordingly to create equivalence ratios (ϕ) of either 1.0 or 4.0 (CH_4/O_2 = 0.5 or 2.0), which correspond to total or partial oxidation. Given the tortuous 80-ppi catalyst geometry with about 83% porosity,[12] steady-state GHSV ranged from 4.0×10^5 to 7.3×10^5 h^{-1}.

Experimental procedures were previously described.[10] Initially, an ambient mixture of methane and air was fed to the reactor at combustion stoichiometry. A spark ignited the mixture, forming a premixed flame upstream of the catalyst that heated the foam monolith to catalytic lightoff ($T > 500$°C) in seconds. After the combustion phase (1 to 20 s in this study), the methane/oxygen ratio was increased to partial oxidation stoichiometry, which extinguished the flame and caused immediate autothermal syngas production. Experimental variability was determined by repeating experiments five times at each combustion time for each flow rate. A total of nearly 50 monoliths were used in this work with reproducible results.

Determination of QMS system response time

Accurate measurement of transient species compositions leaving the reactor required that the response time of the analytical system was rapid and axial mixing of the products was minimized. Quantification of the product response and lag times from the reactor outlet to the QMS system was determined through a set of diagnostic experiments performed under both room temperature and steady-state reactor temperature conditions. First, a mixture at CPO stoichiometry (5 to 15 slpm) was fed to the cold reactor, step changes in each component (CH_4, O_2, Ar) were made sequentially, and the QMS responses were recorded. Figure 2 shows the mass flow controller and QMS system responses to a step change in methane flow rate. Note that there are three time constants involved in the QMS system (mass flow controller response, pre-chamber mixing, and QMS chamber mixing). However, the pre-chamber mixing response (at 0.07 kPa) dominates the QMS chamber mixing response (at 10^{-8} kPa).

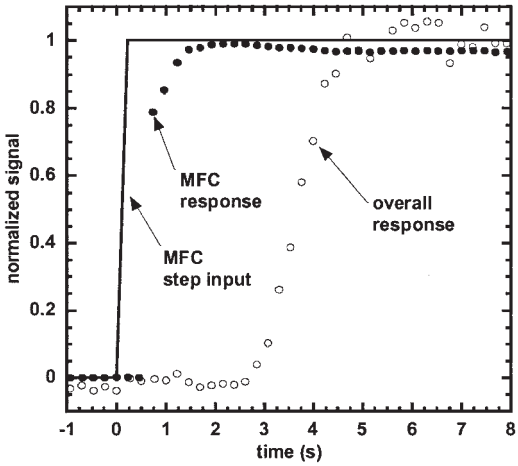

Figure 2. Normalized response of mass flow controller (MFC) and QMS system to step change in methane flow rate.

At $t = 0$ s, a step change from 0 to 5 slpm methane is made (denoted by the solid line) to a steady 5 slpm argon flow, giving 10 slpm total flow at steady state. An initial lag (0.3 s) in the MFC response is followed by an approximately 1.5-s total response time. The total analytical system response (MFC plus QMS) is about 2.5 s after an initial lag time of 2.6 s.

To ascertain an individual response time constant for the QMS system, the mass flow controller response was removed from the overall measured response. Mass flow controller response times were calculated using a first-order fit of the output voltage vs. time. Differences in mass flow controller response time constants between species or flow rates were insignificant (0.53 s average ± 0.11 s standard deviation). A second-order plus time delay model was used to fit the overall measured response, and error was minimized in a least-squares sense. Lag time was determined visually. The fit was calculated by holding one time constant at the predetermined flow controller value while calculating the other. Model fit was excellent for all cases giving a QMS time constant that was not statistically significant between species or flow rates. There was no significant difference between the QMS system response (0.55 s average ± 0.10 s standard deviation) and the flow controller response reported above. A plot of inverse flow rate vs. lag time was linear, as expected.

The above procedure was repeated under steady-state CPO conditions (~ 750°C and 1.1 atm) for the same flow rates (5–15 slpm) for a step change in argon flow rate. Although lag times substantially decreased (the product flow rate under CPO conditions increased nearly fourfold over the reactant flow

rate), the change in the QMS response time constant was statistically insignificant compared to that of previous experiments under room-temperature conditions. This observation indicated that the effect of axial mixing on system response time was insignificant compared to the prechamber mixing response.

Numerical simulations

Numerical computations were used to test the capability of a multistep elementary kinetic model to accurately simulate species profiles during the transient lightoff of methane on Rh for an experimental GHSV of 4.0×10^5 h^{-1} (total inlet flow = 7.1 slpm) and combustion times of 1 and 5 s. A single straight hypothetical pore of a 5-mm-long 80-ppi foam monolith was modeled using a nominal diameter of 0.25 mm, effectively neglecting the tortuous pore network found in ceramic foams. To generate numerical species profiles, model feed conditions were matched to the recorded mass flow controller outputs from experiment at time t. Simulations in this work used a one-dimensional (1D) plug-flow model with a detailed 38-step surface chemistry mechanism for methane oxidation on Rh.[9] Gas-phase chemistry is negligible at low-pressure conditions for methane CPO[13-15] and was not included in the simulations.

The plug-flow species continuity equations can be written as

$$\rho u A \frac{dY_k}{dz} + Y_k a_i \sum_{gas}^{K_g} \dot{g}_k W_k = W_k(\dot{g}_k a_i + \dot{\omega}_k A) \qquad (1)$$

where ρ is the mass density and u is the axial velocity of the gas, which consists of K_g species; W_k is the molecular weight of species k and $\dot{g}_k$ is the molar production rate of species k by all surface reactions. Y_k is the mass fraction of species k and $\dot{\omega}_k$ is its molar production rate by gas-phase chemistry. A and a_i are the cross-sectional area and internal surface area per unit length of reactor, respectively. The catalyst's activity is included through the assumed site density for the Rh surface, which was 2.9×10^{-9} mol/cm^2 for the mechanism. The differential algebraic equations resulting from the plug-flow treatment were solved using the CHEMKIN PLUG code.[16]

The plug-flow assumption was verified using two criteria. If only radial mass transfer is considered, then plug flow can be assumed if

$$\mathrm{Fo} = \frac{D\theta}{r^2} > 1 \qquad (2)$$

where Fo is the Fourier number, D is the characteristic diffusion coefficient, θ is the residence time, and r is the reactor radius.[17] A more complete assessment treating both the axial and radial transport assumptions of plug flow yields the following acceptable bounds:

$$\frac{d}{L} \ll \mathrm{Re}_d \mathrm{Sc} \ll \frac{L}{d} \qquad (3)$$

where d is the reactor diameter, L is the reactor length, Re_d is the Reynolds number based on reactor diameter, and Sc is the Schmidt number.[18] Using Eq. 3, a 5-mm catalyst length and 0.25-mm pore diameter give a practical range of 0.05–20 for the mass transfer Peclet number. The CHEMKIN module TRANSPORT[19] was used to calculate binary transport coefficients based on temperature and species, whereas a mixture average treatment was used to calculate characteristic transport coefficients for Eqs. 2 and 3. Based on the average GHSV and stoichiometry used in this study (4×10^5 h^{-1} and CH_4/O_2 = 0.5–2.0) and assigned temperature history of the catalyst, which is presented in the next section, the radial mass transfer Fourier number ranged from about 2 to 25, whereas the mass transfer Peclet number range was 2–9 over the transient lightoff period, thus validating the plug-flow assumption.

Under the experimental conditions used, reactor residence times of 1 to 10 ms are typical and can be considered a representative timescale for reactive flow. A more relevant timescale for surface chemistry would be Rh surface desorption times for pertinent species at 1000 K that range from approximately 10^{-3} to 10^{-12} s (for example, 10^{-3} s for O_2, 10^{-9} s for H_2, and 10^{-12} s for H_2O). However, the reaction timescales are many orders of magnitude smaller than the monolith thermal response time, O(1 s). Therefore, the timescales for reactive flow and catalyst thermal response are assumed decoupled in these simulations. Taking advantage of this simplification, transient temperature profiles were used in the simulations so the energy equation was not solved.

Temperature profiles for numerical simulations

Because a premixed flame initially heats the catalyst, only by solving the Navier–Stokes equations with homogeneous chemistry and radiation treatment can a rigorous numerical solution for the transient catalyst temperature profile be attained after the combustion phase. To simplify the model, all uncertainty about the axial temperature profile in the first few seconds of lightoff was placed into parameterized catalyst temperature profiles, which were used in simulations.

To isolate parameters for the temperature profiles, previous experimental and numerical investigations focusing on the monolith temperature profile under steady-state and transient CPO conditions were examined. At steady-state CPO conditions similar to conditions in this work, the maximum catalyst temperature (1200°C) is found within the first millimeter of the monolith[20] and is indicative of a short, exothermic oxidation section where oxygen is completely consumed. The endothermic reforming section after the first millimeter is characterized by a roughly exponential temperature decrease to the catalyst back face ($\sim$ 400°C temperature drop); a linear temperature decrease of about 300°C is observed from 1 to 5 mm.[20] Data from previous lightoff experiments and simulations suggest that for very short initial combustion times ($\sim$ 1 s), no temperature overshoot (compared to the steady-state profile) occurs.[10] For slightly longer combustion times (such as 5 s), temperature overshoot presumably occurs in the oxidation section, and for even longer combustion times it can occur in the reforming section. To determine the kinetic model's ability to reproduce experimental species profiles with and without the overshoot phenomena, both 1- and 5-s combustion time temperature profiles were developed.

Based on the above considerations, three parameters were used to generate the temperature profiles for the 1-s combustion time model: (1) steady-state catalyst front-face temperature; (2)

oxidation section length (ℓ_{ox}); (3) heating time constant for the catalyst front face ($\tau_{ff,h}$). Because radial mixing is pronounced in the foam, temperature was lumped in the radial direction and distributed axially. A first-order exponential heating profile was used to estimate how the front-face temperature developed. The oxidation section length was made isothermal for simplicity and assumed to develop instantaneously in space at the feed switch. The remainder of the catalyst temperature profile, which simulates the reforming section, followed an exponential decay to the experimentally measured back-face temperature at each time point

$$T(z > \ell_{ox}, t) = T(z, 0) + [T(0, t) - T(z, 0)]\exp\left[\frac{z - \ell_{ox}}{\tau_s(t)}\right] \quad (4)$$

where $T(z, 0)$ is the initial monolith temperature from experiment and $T(0, t)$ is the front-face temperature at time t. The spatial decay constant $\tau_s(t)$ was determined by inserting $T(z, 0)$ and $T(0, t)$ into Eq. 4 and solving for the value of $\tau_s(t)$ to make $T(5\text{ mm}, t)$ equal to the measured back-face temperature at time t. The spatial decay constant at each time point was completely defined by the catalyst front-face temperature, oxidation section length, and measured back-face temperature, and was not an independent parameter.

For the 5-s combustion time model, two additional parameters were used because temperature overshoot occurred in the oxidation section based on experimental results. These parameters were the theoretical overshoot temperature in the oxidation section at 5 s (T_{max}), and the front-face cooling time constant ($\tau_{ff,c}$), which was applied in simulations at the catalyst front face after 5 s to lower the front-face temperature to its steady-state value.

Optimized values for the oxidation section length and steady-state front-face temperature were determined by minimizing the least-squares error between simulation output and averaged steady-state species data. Optimized values for the remaining parameter(s) for the 1- and 5-s combustion time models were obtained by fitting the transient simulation output to experimental data in a least-squares sense for the 1-s combustion time case and visually for the 5-s combustion time case.

Results

First, experimental findings for product species profiles and catalyst temperature are presented for 1- to 20-s combustion times and various feed flow rates. Next, the general behavior of the surface chemistry mechanism used in simulations is outlined over a range of experimentally relevant temperatures. Last, results from plug-flow simulations incorporating the transient temperature profiles are compared to combustion time experiments of 1 and 5 s.

Temperature and species profiles for short combustion times

For a 5 slpm air flow rate, species profile results from experiments using 1- and 5-s combustion times are shown in Figure 3. Similar trends exist for both 1- and 5-s combustion time experiments. Standard deviations of approximately 5–10% of the local 1-s average are found for each species. Upon sparking the combustion mixture ($t = 0$ s), oxygen and methane flow rates rapidly decrease toward zero, whereas carbon dioxide begins to increase. Hydrogen and carbon monoxide production is near zero. The catalyst back-face temperature rises rapidly after a nearly 2-s delay. Upon switching to CPO stoichiometry, methane flow is increased fourfold, whereas air flow is held constant. After this feed switch, hydrogen and carbon monoxide flow rates start to rapidly increase. Note that the methane mass flow controller response time for 99% gain is about 2 s and contributes to the observed delay. The carbon dioxide flow rate peaks immediately after the switch and then decreases to its steady-state CPO value. Oxygen flow remains at zero, whereas the methane flow reaches a minimum near zero then increases to its new steady-state value. Steady-state back-face temperatures are in the range of 700–750°C.

However, significant differences in species response exist between the two combustion times. For a nearly 1-s combustion time (Figures 3A and B), overshoot occurs in the methane flow upon switching to $\phi = 4.0$, indicating breakthrough and that catalyst preheat was below optimum (undershoot in catalyst temperature compared to steady-state CPO conditions). Temperature, hydrogen, carbon monoxide, and methane reach their steady-state values within 15–20 s. A 5-s combustion time (Figures 3C and D) proves much more effective in producing a quick steady state for syngas. Hydrogen and carbon monoxide reach steady state within 10 s (within 5 s from the switch), and the temperature monotonically increases to steady state. A slight overshoot in carbon monoxide at the feed switch indicates that a temperature overshoot in the catalyst may occur during the combustion phase. The methane behavior indicates that the front portion of the catalyst possesses a higher temperature for the 5-s combustion time than the 1-s combustion time upon feed switch. Methane does not exhibit breakthrough as in the 1 s case and instead rises smoothly to steady state (Figures 3C and D).

A comparison of the transient fuel conversion and syngas selectivities marks the difference between 1- and 5-s combustion times more clearly (Figure 4). For the 1-s combustion time, methane conversion peaks near 100% at 2 s during the combustion phase (Figure 4A). Once the stoichiometry is switched, fuel conversion drops to below 60% then slowly rises back to a steady-state conversion of about 70%. Approximately 85% carbon monoxide and hydrogen selectivities are reached within 15 s. Using a 5-s combustion time initially gives nearly 100% fuel conversion from 3 to 5 s (Figure 4B). Upon switching the feed composition, methane conversion quickly decreases to 70%, exhibiting no breakthrough compared to steady-state performance. Selectivities to hydrogen and carbon monoxide increase to about 85% within the same time span.

Experiments performed with 7 and 9 slpm air flow rates give the same general results, although peak back-face temperatures increase over the 5 slpm air flow experiment, as expected. For this reason, combustion times > 10 s were not performed with these higher flows because the peak back-face temperature for 10-s combustion time experiments exceeded 1200°C, risking Rh sintering and pronounced metal migration. A 5-s combustion time for 7 and 9 slpm air flow rates yields steady-state syngas selectivities of 85% within 10 s (data not shown).

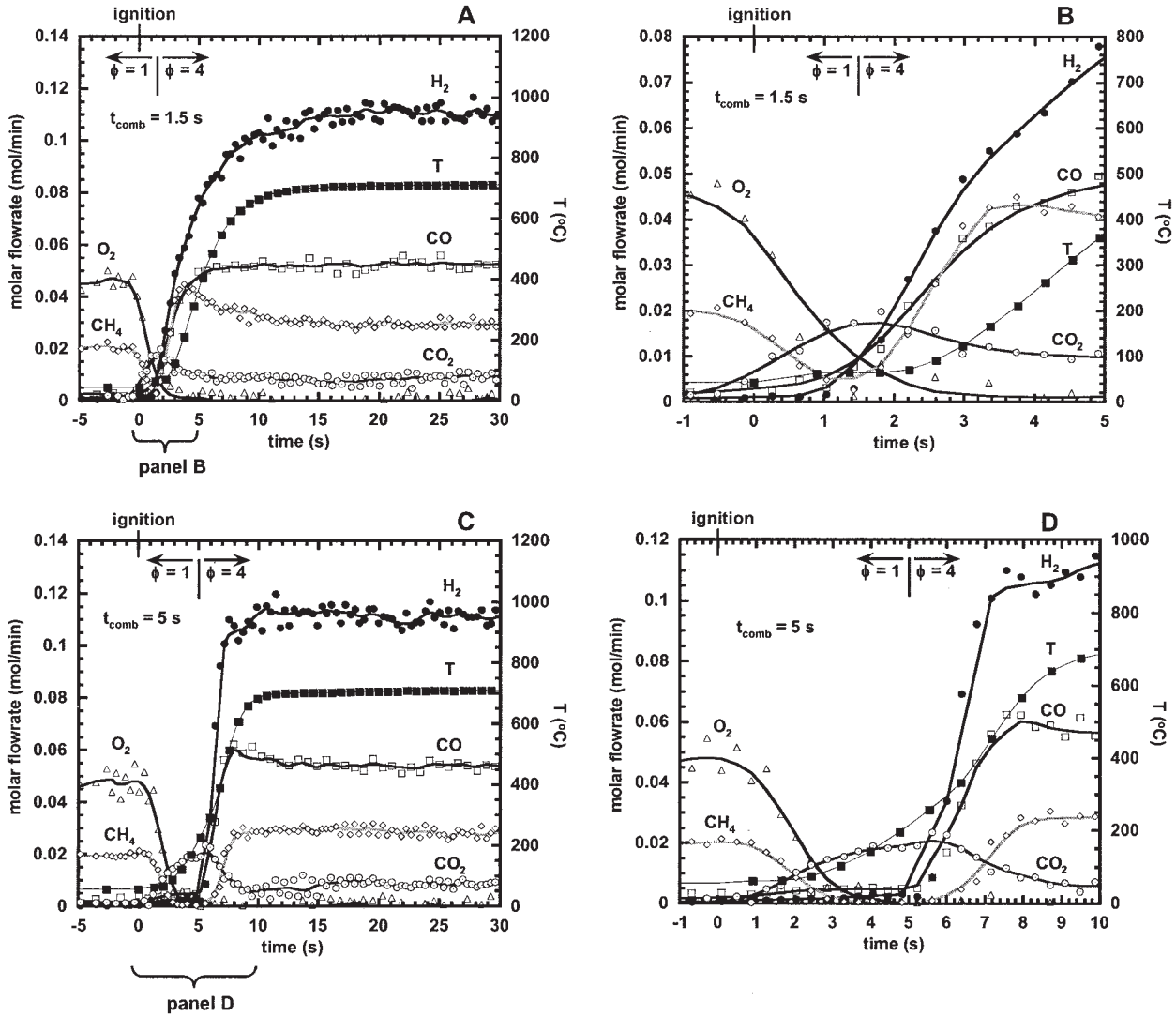

Figure 3. Effect of short combustion times on product flow vs. time for 5 slpm air flow rate on a 5-mm Rh catalyst.

Markers represent output from the QMS system with lag time removed, whereas lines are a locally weighted least-squares fit to the data. Ignition of the combustion mixture occurs at $t = 0$ s. (A) Combustion time of about 1.5 s. (B) Magnified view for combustion time of about 1.5 s over −1 to 5 s. (C) Combustion time of 5 s. (D) Magnified view for 5-s combustion time over −1 to 10 s.

Steady-state fuel conversions (~ 70%) are also similar to the lower flow rate experiments.

Temperature and species profiles for longer combustion times

For combustion times ≥ 10 s, back-face temperature overshoots steady state and is accompanied by pronounced overshoot in hydrogen and carbon monoxide after the feed composition is switched (Figure 5). As combustion time is increased from 10 to 20 s, back-face temperature and CPO product overshoot become more dramatic. These phenomena indicate that the catalyst becomes increasingly superheated with increasing combustion times compared to the temperature profile for steady-state partial oxidation. Longer combustion times decrease the initial hydrogen and carbon monoxide response times and increase the response time for unconverted methane to rise to its steady-state value.

General behavior of the kinetic mechanism at steady state

Figure 6 displays isothermal catalyst performance for the detailed surface chemistry mechanism[9] over the range of temperatures typically found in a lightoff sequence and GHSV applicable to this study ($2.0–7.3 \times 10^5$ h^{-1}) and equilibrium data. Equilibrium values were calculated using the CHEMKIN module EQUIL, which minimizes the Gibbs free energy of the chemical system.[21] Three distinct kinetic regimes are evident in this mechanism. In the first regime, the catalyst lights off between 420 and 500°C, yielding combustion products (CO_2 and H_2O). The second regime (between 500 and 700°C) gives mostly combustion products. Methane conversion is approximately constant (~ 25%) in this regime because methane is fed in excess of combustion; oxygen conversion is complete after 500°C. In the third regime (>700°C), syngas quickly becomes the major product as temperature and methane conversion

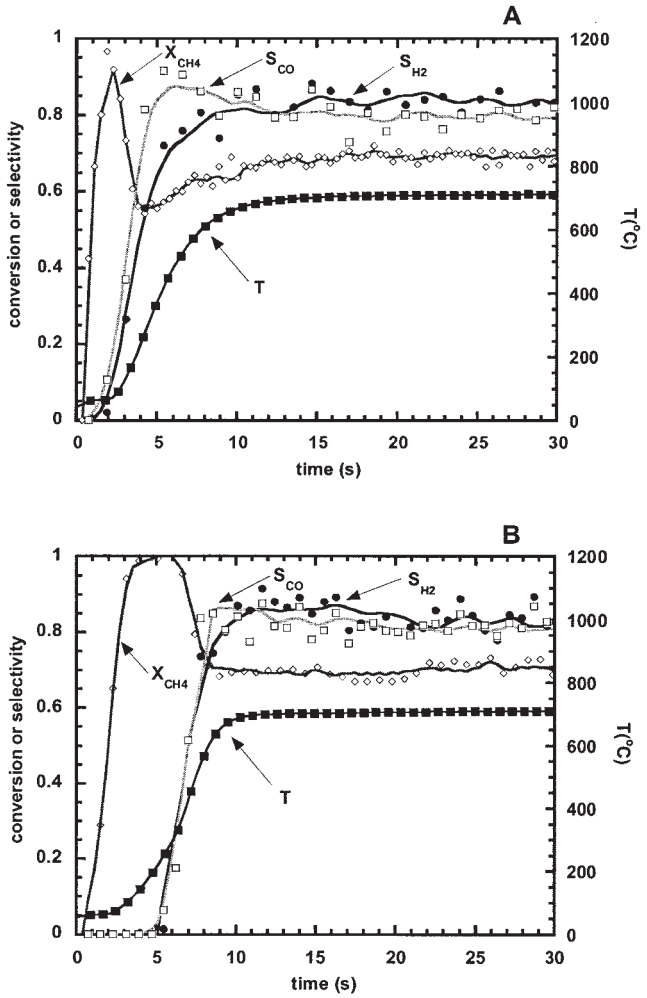

Figure 4. Effect of combustion time on CH_4 conversion (X_{CH4}) and syngas selectivities (S_{CO} and S_{H2}) vs. time for 5 slpm air flow rate on a 5-mm Rh catalyst.

Markers represent output from the QMS system with lag time removed, whereas lines are a locally weighted least-squares fit to the data. Ignition of the combustion mixture occurs at t = 0 s. (A) Combustion time of 1 s. (B) Combustion time of 5 s.

increase. At the highest temperatures, the lowest space velocity (2.0×10^5 h^{-1}) gives product compositions that approach equilibrium composition.

Temperature and species profiles for short combustion time simulations

Table 1 summarizes the optimized parameters for the 1-s combustion time temperature profile. Results from the 1-s combustion time simulation (Figures 7 and 8) show that a transient, distributed temperature profile can be combined with steady-state chemistry to reproduce experimental profiles. The temperature of the catalyst oxidation section quickly rises in the first second (Figure 7A) above the lightoff temperature for methane on Rh ($\sim$ 500°C). Upon switching to CPO conditions after about 1.5 s, the catalyst front face heats further, albeit at a slower rate, to steady-state CPO temperature. The temperature difference between the front and back of the catalyst peaks after a few seconds and then slowly decays to its 200°C steady-state value, which effectively mimics transient heat transport to the catalyst back face. The combination of the

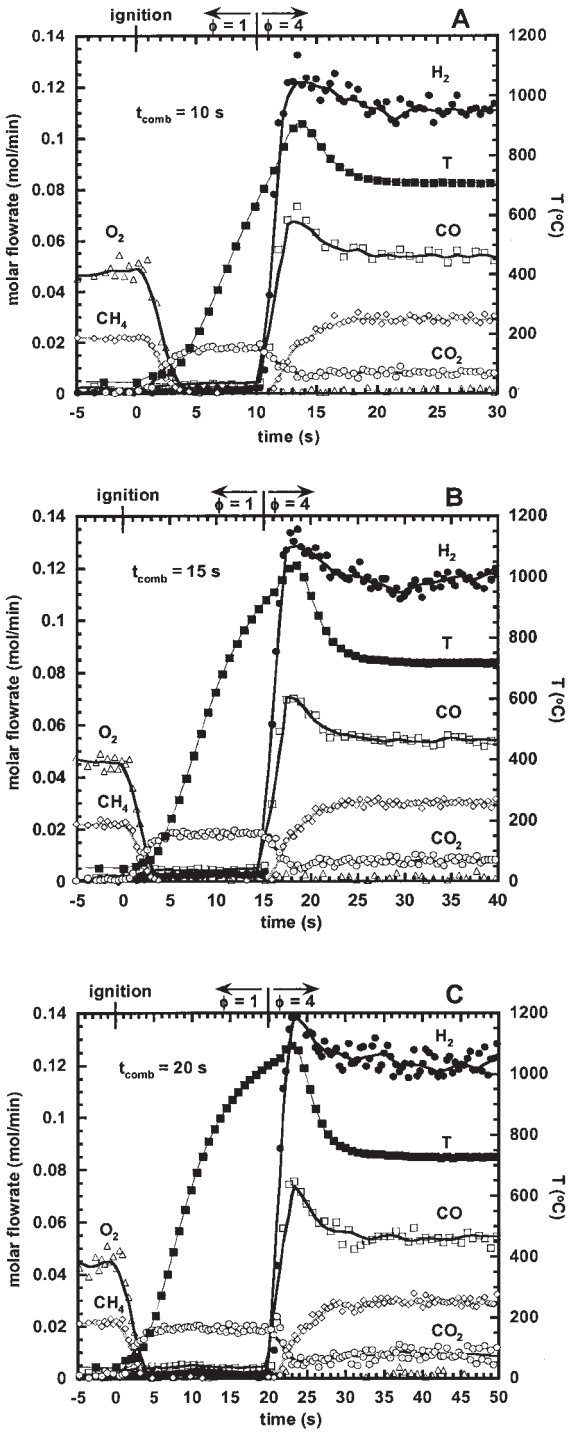

Figure 5. Effect of longer combustion times on product flow rates vs. time for 5 slpm air flow rate on a 5-mm Rh catalyst.

Markers represent output from the QMS system with lag time removed, whereas lines are a locally weighted least-squares fit to the data. Ignition of the combustion mixture occurs at t = 0 s. (A) Combustion time of 10 s. (B) Combustion time of 15 s. (C) Combustion time of 20 s.

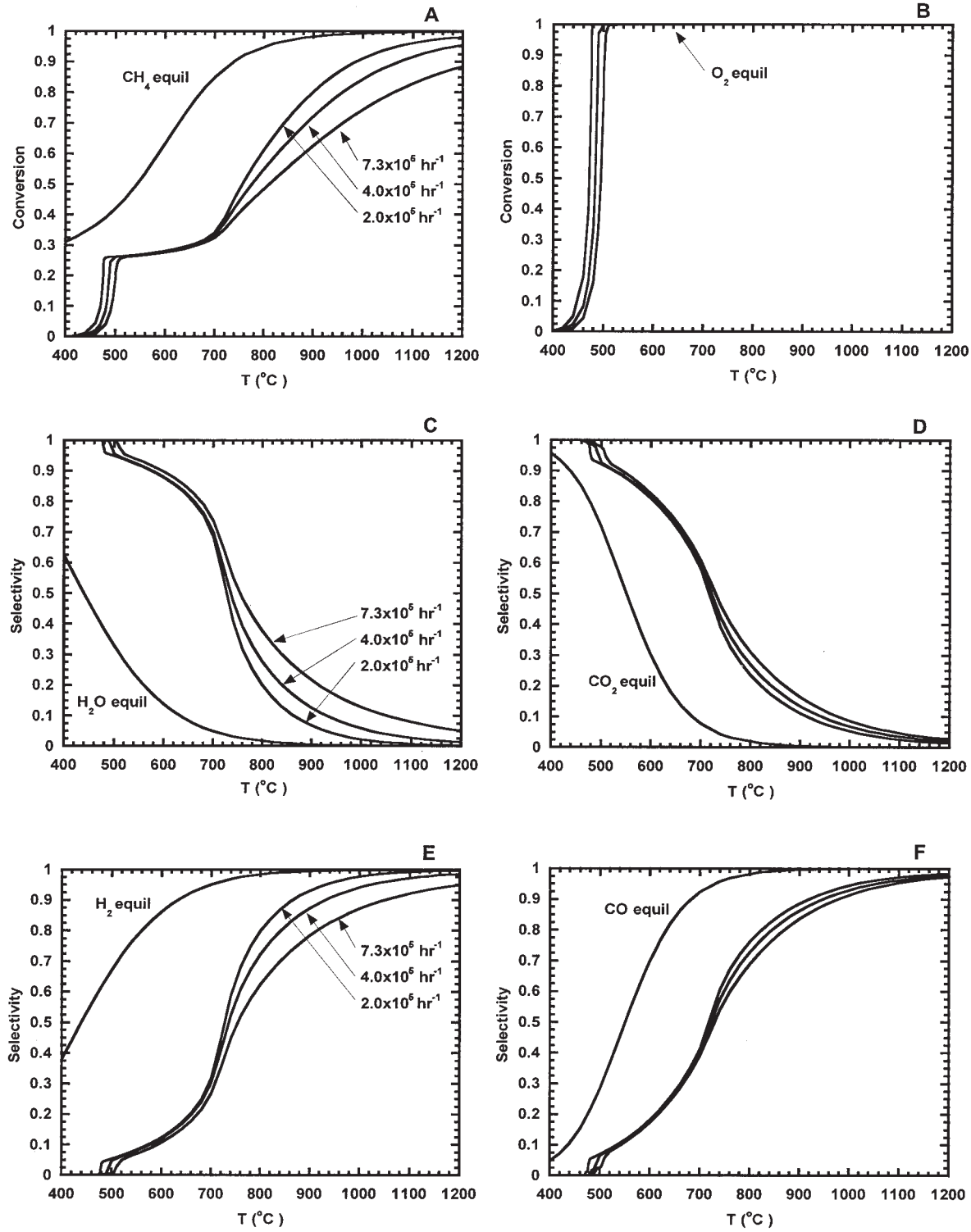

Figure 6. Steady-state conversions and selectivities vs. isothermal reactor temperature for an atmospheric plug-flow simulation with a methane/air feed at $\phi = 4.0$.

Results are shown for GHSV relevant to this study and equilibrium. In each row, GHSV values denoted in the left panel also correspond in the same trend to the data in the right panel. (A) Methane conversion. (B) Oxygen conversion (note that equilibrium oxygen conversion is 100% from 400 to 1200°C for $\phi = 4.0$). (C) Water selectivity. (D) Carbon dioxide selectivity. (E) Hydrogen selectivity. (F) Carbon monoxide selectivity. The simulations show catalyst lightoff at low temperatures (420 to 500°C), combustion products (carbon dioxide and water) at moderate temperatures (500 to 700°C), and partial oxidation products (hydrogen and carbon monoxide) at high temperatures (>700°C). At high temperatures, the product profiles approach equilibrium as GHSV decreases (residence time increases).

Table 1. Temperature Profile Parameters for 1-s Combustion Time Simulation

Input parameters	
Oxidation section length	1 mm
Catalyst ΔT at steady state	200°C
$\tau_{ff,h}$*	1.1 s
T (5 mm, t)	Experimental value
Profile summary	
T (0–5 mm, 0 s)	40°C
T (0–1 mm, ∞)	915°C
T (5 mm, ∞)	715°C

*Oxidation section heating time constant.

oxidation section temperature, experimental catalyst back-face temperature, and exponential decay for the remainder of the catalyst simulates the temperature development of the reforming section in time and space after the stoichiometry switch (Figure 7B). Physically, the temperature drop in the reforming section is initially attributed to latency in heat transport, whereas at steady state it is caused by endothermic reactions.

The first 1 s of the experiment cannot be rigorously compared to the model because fuel consumption is likely all

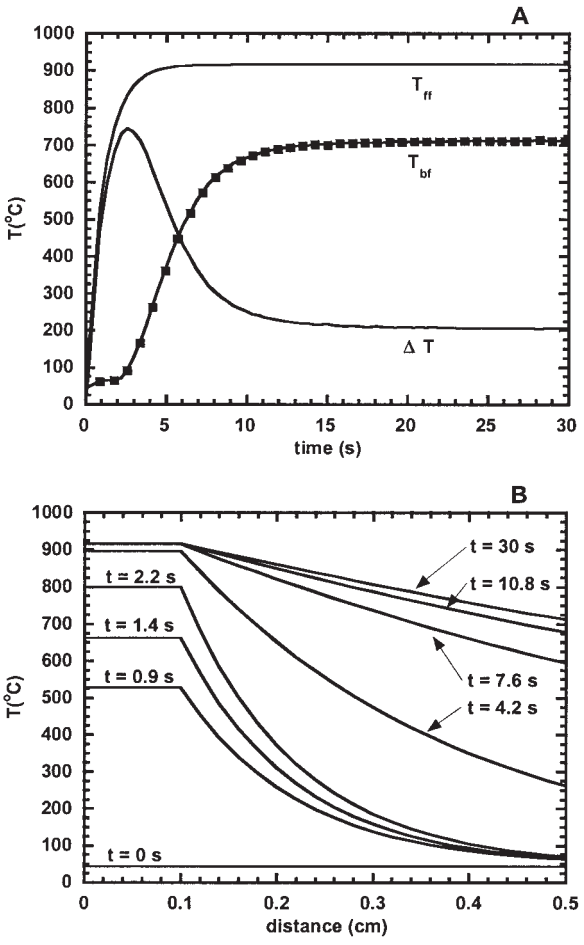

Figure 7. Temperature profiles for 1-s combustion time simulation.

Profile parameters are given in Table 1. (A) Assumed catalyst front-face temperature (T_{ff}) and experimental back-face temperature (T_{bf}) vs. time. The first 1 mm of the catalyst (oxidation section) experiences first-order heating and reaches steady-state temperature in about 5 s. (B) Combining the front- and back-face temperature profiles with an exponentially decaying profile for 1–5 mm (reforming region) gives an axially distributed, transient temperature profile for the 5-mm catalyst.

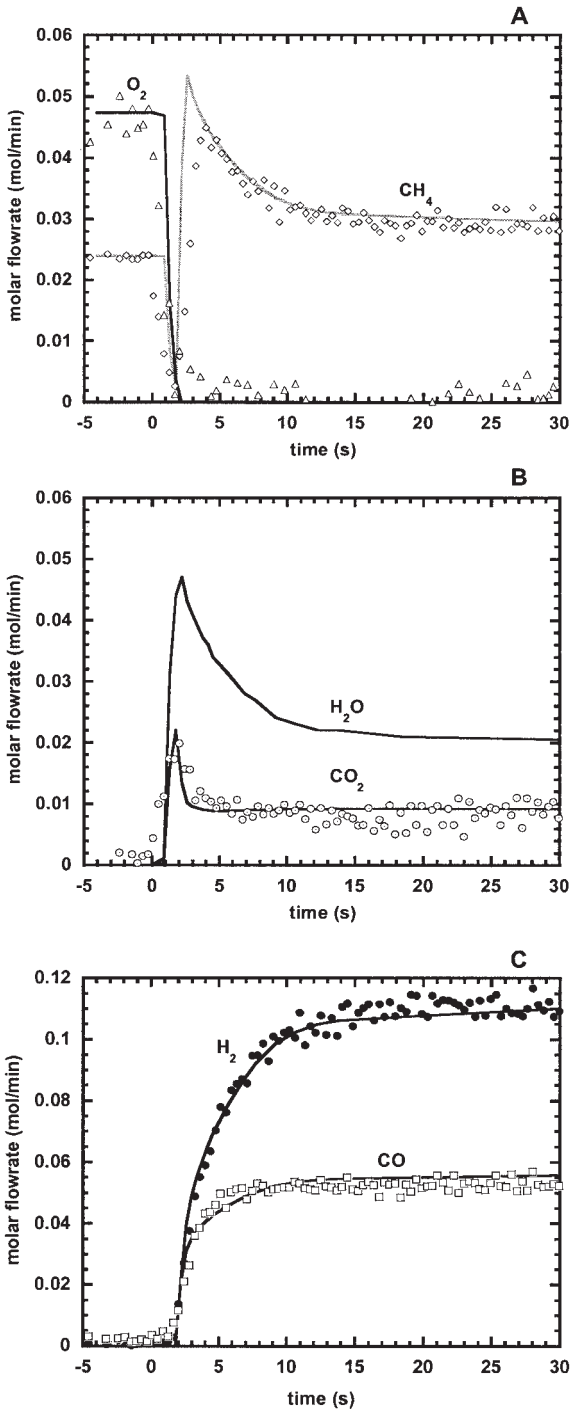

Figure 8. Transient species profiles for 1-s combustion time simulation.

Experimental species profiles (markers) and numerical profiles (solid lines) for (A) methane and oxygen; (B) carbon dioxide and water (only simulation shown); (C) hydrogen and carbon monoxide. The model captures the transient profiles after switching the feed stoichiometry at 1.5 s.

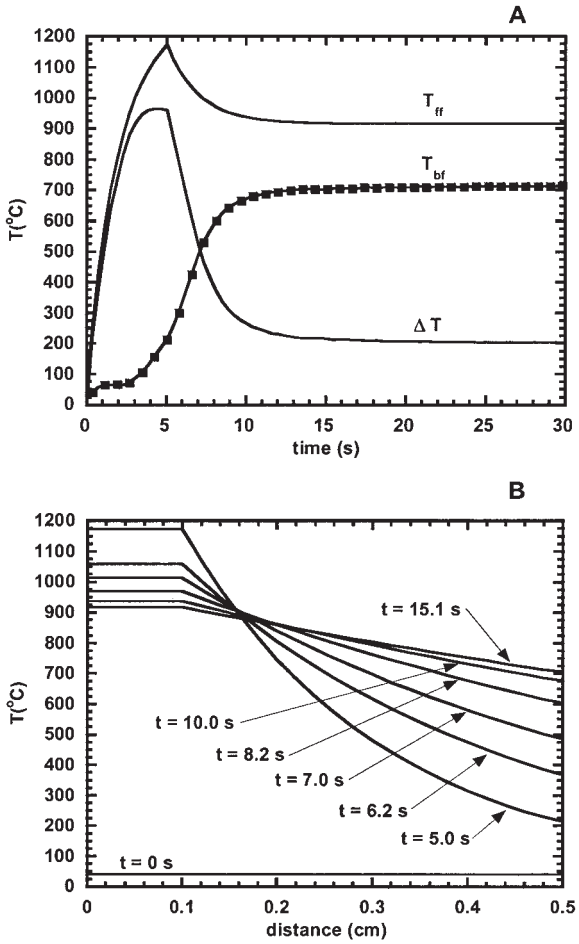

Figure 9. Temperature profiles for 5-s combustion time simulation.

Profile parameters are given in Table 2. (A) Assumed catalyst front-face temperature (T_{ff}) and experimental back-face temperature (T_{bf}) vs. time. The first 1 mm of the catalyst (oxidation section) experiences first-order heating (0 to 5 s) then cooling (5 to 13 s) to its steady-state temperature. Note that the oxidation section temperature for this profile is consistent with the 1-s combustion model through the first 1.5 s. (B) Combining the front- and back-face temperature profiles with an exponentially decaying profile for 1–5 mm (reforming region) gives an axially distributed, transient temperature profile for the 5-mm catalyst.

homogeneous in experiments yet heterogeneous in simulations. However, good agreement is still found in both fuel conversion (Figure 8A) and carbon dioxide production (Figure 8B). Upon switching to CPO conditions at 1.5 s, the simulation qualitatively predicts the methane breakthrough experimentally observed. Experimental and simulated peak methane breakthrough values are not the same; however, the comparison is not entirely valid until the transition from $\phi = 1.0$ to 4.0 is complete, and the upstream flame is extinguished (at $\sim$ 2–3 s). In addition, the QMS system may not be able to resolve the rapid methane breakthrough peak that occurs in less than 2 s. After 4 s, simulated and experimental methane conversions match well. Transient and steady-state agreements are excellent between model and experiment in syngas production, which occurs after 3 s (Figure 8C).

To test the temperature profile assumptions for longer combustion times, simulations were also performed for the 5-s combustion time case. In the first 5 s of lightoff, the oxidation section reaches a maximum temperature that overshoots steady-state CPO conditions (Figure 9A). The oxidation section heating profile is equivalent to the heating profile for the 1-s combustion model over the first 1.5 s to maintain consistency between both models. After 5 s, the oxidation section experiences first-order cooling to the steady-state CPO temperature from the 1-s model. As in the 1-s combustion simulation, an exponentially decaying profile for the catalyst from 1 to 5 mm is coupled with the assumed oxidation section temperature profile and experimental back-face temperatures to simulate the reforming section's thermal history (Figure 9B). Temperature profile parameters for the 5-s model are shown in Table 2. For this case, simulated species profiles are shown only after 5 s because the simulated and experimental chemistry would be fundamentally different between 0 and 5 s.

Upon switching to CPO feed at 5 s, methane flow does not exhibit overshoot in experiments (as in the 1-s combustion time case). Instead, it slowly approaches its steady-state value (Figure 10A). This phenomenon is consistent with a superheated catalyst front section as assumed in the temperature profile and reflected in the simulation. However, the simulation predicts a quicker response than experiments show for both methane and carbon dioxide (Figures 10A and B). This response disparity is also noticeable for hydrogen and carbon monoxide production (Figure 10C). The simulation predicts overshoot in both hydrogen and carbon monoxide, whereas overshoot in only carbon monoxide is found for 5-s combustion time experiments.

Discussion

In this work, rapid startup of a short-contact-time reactor to produce syngas from methane has been demonstrated within a timescale relevant to mobile power applications (5–10 s) and in the absence of any external heating source. The reactor employs a Rh-impregnated ceramic foam monolith and an initial homogeneous combustion phase (duration of 1–5 s) to preheat the catalyst front face above the autocatalytic ignition temperature. Steady-state hydrogen yield is about 60% within 10 s for a CH_4/O_2 ratio = 2.0; yield could be increased significantly by running at a leaner feed composition ($CH_4/O_2 \cong 1.8$), as shown in previous steady-state experiments.[20] Partial oxidation stoichiometry was used only to show proof of concept of the

Table 2. Temperature Profile Parameters for 5-s Combustion Time Simulation

Input parameters	
Oxidation section length	1 mm
Catalyst ΔT at steady state	200°C
$\tau_{ff,h}$*	2.0 s
$\tau_{ff,c}$**	2.0 s
T_{max} (0–1 mm, 5 s)†	1265°C
T (5 mm, t)	Experimental value
Profile summary	
T (0–5 mm, 0 s)	40°C
T (0–1 mm, 5 s)	1166°C
T (0–1 mm, ∞)	915°C
T (5 mm, ∞)	715°C

* Oxidation section heating time constant.
**Oxidation section cooling time constant.
† Theoretical overshoot temperature in oxidation section at 5 s if $\tau_{ff,h} \rightarrow 0$ s.

reactor design. One-dimensional plug-flow simulations of short combustion time experiments (1 and 5 s) demonstrate that transient species profiles can be reproduced using an established surface mechanism typically used to model steady-state chemistry. Combining empirically based assumptions for the thermal catalyst history with the plug-flow model resulted in the development of a transient, axially distributed temperature profile that offers insight into how the catalyst temperature develops during lightoff. This modeling flexibility is realized because the reaction timescales for this process are at least several orders of magnitude smaller than the catalyst temperature response time. Therefore, chemistry and temperature during reactor start-up can be decoupled.

Minimizing startup time by modifying combustion time

Lightoff experiments at a constant 5 slpm air feed elucidated how initial combustion time affects the overall time in which steady-state syngas is obtained. A 1-s combustion time yields steady-state syngas production within nearly 15 s after the switch (Figure 3A). Increasing combustion time to 5 s dramatically decreases syngas response time to 4–5 s (Figure 3C); however, adding the initial 5-s combustion time to the syngas response gives a total duration of 10 s from the start of the experiment. At combustion times of $\geq$ 5 s, the catalyst yields syngas as fast as the mass flow controller can switch the stoichiometry. Because the controller response is about 2 s, any decrease in syngas response time after switching by using combustion times $>$ 5 s cannot be distinguished by the analytical system. If an optimal start-up time is desired, a trade-off exists between the length of combustion time and the catalyst response time after switching to CPO conditions. By using an optimal combustion time, methane breakthrough (at short combustion times) and syngas overshoot (at longer combustion times) are avoided. A combustion time of about 3 s gives steady-state syngas production in $<$ 7 s from the start of the experiment (data not shown), effectively heating the catalyst to a temperature profile similar to the steady-state CPO profile. Initial axial heat transport resistance is hypothesized to facilitate start-up so that by the feed switch, the temperature profile closely matches the steady-state CPO profile, which is characterized by a short, high-temperature oxidation section and a longer, lower-temperature reforming section. At higher feed flow rates (7 and 9 slpm air), the optimal combustion time decreases slightly for the same catalyst dimensions because of larger heat release.

Hydrogen response time in the QMS

Concern over longer hydrogen response compared to that of other species and its effect on the accuracy of the transient profiles is warranted. Gases used in QMS diagnostic analyses had molecular weights $\geq$ 16. Hydrogen poses a greater challenge for rapid QMS response. The hydrogen pumping speed of a turbomolecular pump is typically determined by the relatively low compression ratio since the natural logarithm of the compression ratio is proportional to the square root of the gas molecular weight. The importance of this issue can be ascertained by analyzing transient hydrogen selectivity from experiments. For a 1-s combustion time (Figure 3A), experimental hydrogen and carbon monoxide response times after feed switch are comparable ($\sim$ 10 s) and much longer than the QMS system response times measured in diagnostic work. Therefore, accurate results are ensured. In longer combustion time experiments, overshoot in syngas is quickly observed (Figure 5). Peak hydrogen selectivity is 80–90% after feed switch (based

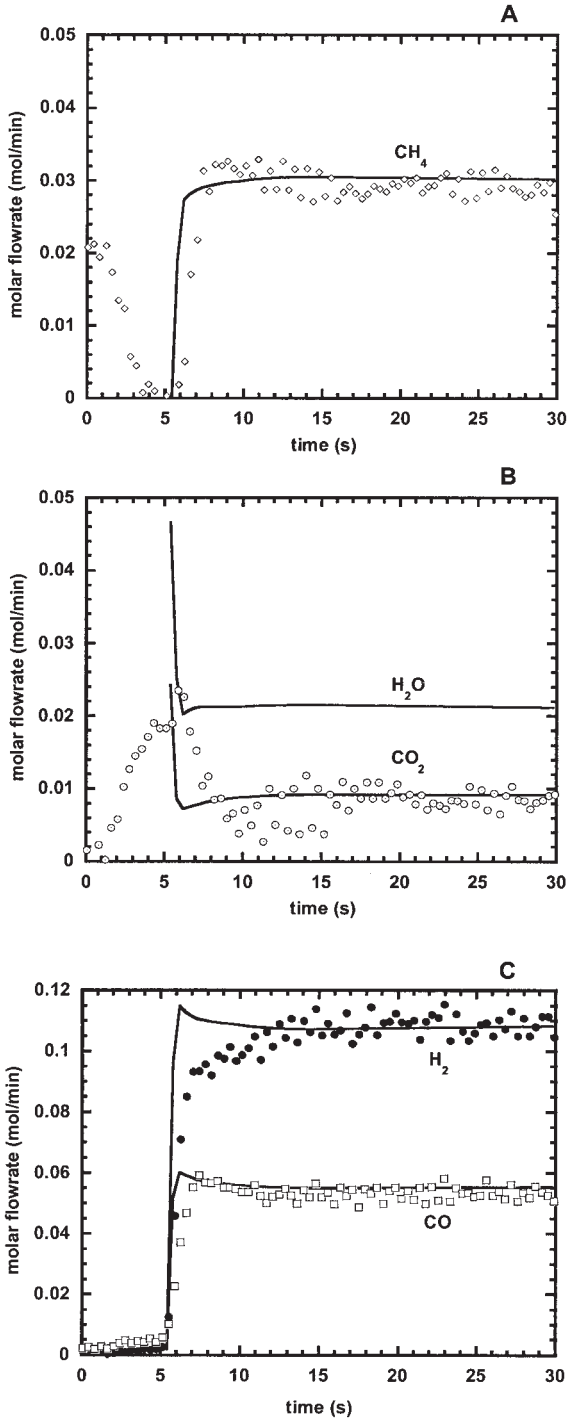

Figure 10. Transient species profiles for 5-s combustion time simulation.

Experimental species profiles (markers) and numerical profiles (solid lines) for (A) methane; (B) carbon dioxide and water (only simulation shown); (C) hydrogen and carbon monoxide.

on methane input), demonstrating that the QMS system may not accurately resolve the large spikes in hydrogen production upon adjusting the feed composition. However, these inconsistencies in the hydrogen balance are found only at the peak response for longer combustion time experiments. The QMS response may also explain the initial quantitative discrepancies between experimental and simulated methane breakthrough peaks for the 1-s combustion time case (Figure 8A) and experimental and simulated carbon monoxide and hydrogen peaks for the 5-s combustion time case (Figure 10C).

Catalyst deactivation

Fast lightoff experiments have been conducted using 50 monoliths with reproducible results. For individual monoliths, no significant difference is found in catalyst performance over 20 lightoff sequences at the flow rates presented in this work as long as combustion times < 10 s are used. At longer combustion times, some deterioration in syngas yield and catalyst mechanical integrity is observed after as few as 5 lightoff experiments. At longer combustion times, Rh in the catalyst front section reaches temperatures well above 1200°C causing sintering and metal migration and agglomeration that decrease the active catalyst area and effective catalyst length. However, catalyst deterioration at long combustion times is not an issue because combustion times > 5 s are not needed to rapidly effect syngas production.

Kinetics and transport phenomena in methane CPO

The kinetic mechanism used in this study does not predict equilibrium products over the majority of the temperature range of interest in this study, as shown in Figure 6. There has been considerable debate on the role of transport phenomena in methane CPO on Pt and Rh. Previous experimental and numerical efforts with Rh and Pt foams suggest that the system is flux limited by methane adsorption rather than by external mass transfer through a boundary layer, given that foams have very high interphase mass transfer rates.[2,15] This phenomenon is manifested by the very small sticking coefficients used for methane adsorption in the mechanisms mentioned above and the similar mechanism used in this study.

However, a performance comparison of several multistep mechanisms for methane oxidation with in situ experimental observations indicated a large uncertainty for the methane adsorption sticking coefficient on Pt.[22] For fixed-bed supports, experimental and numerical studies with Rh-coated sphere beds have suggested that the process is oxygen mass transfer limited through a boundary layer.[23,24] However, surface adsorption steps were not considered in the simulations. A more detailed numerical study of Rh-coated fixed beds using the same mechanism as in this work concluded that the importance of external mass transfer compared to methane adsorption increased with GHSV and particle size.[25]

The studies presented above for methane CPO on Pt and Rh agree on the qualitative details of the catalyst's axial temperature and species profiles at steady state, regardless of support structure. The catalyst entrance or oxidation section is characterized by a maximum temperature where oxygen is completely consumed by both total and partial fuel oxidation. The remaining section of the catalyst allows endothermic reforming reactions (CO_2 and H_2O reacting with the remaining fuel) and possesses a monotonic decrease in temperature.

Transient simulations

The goal of the transient models was to investigate how the axial temperature of the monolith may develop during lightoff by simulating a single hypothetical pore of the foam catalyst. In reality, foam monoliths are a highly porous and tortuous network of interconnected cells with a distribution of pore sizes unlike that of traditional honeycomb monoliths. Honeycomb structures consist of straight parallel channels of well-defined and uniform cross section that are segregated convectively yet linked thermally. Modeling the lightoff of honeycomb structures has shown great promise[9] and benefits from the clearly defined geometry. These structures offer fertile ground for computational fluid dynamics model development of catalytic structures. Experimentally, however, many chemical reaction processes perform better with foam structures than with conventional sphere beds and honeycomb structures. Foams offer benefits over conventional supports such as pronounced radial mixing, lower pressure drop, and higher effectiveness factors,[12] although the heat transfer properties of sphere beds allow them to operate at higher GHSV without blowout for methane CPO.[26]

The foam monolith geometry is quite complex, random, and therefore ill-defined for rigorous computational mesh development. However, assuming the development of a computational mesh possessing this intricate pore structure, accurate solution of the conservation equations coupled with even a simplified chemistry mechanism would be intractable with current computational resources considering the mesh refinement necessary. In contrast, solution of the energy equation with transport treatments more complex than that of plug flow is of little quantitative benefit to intra-catalyst study if a pore is approximated as a single, straight channel because critical aspects of the foam geometry are ignored. If the averaged effluent species compositions are of primary concern, the high degree of radial mixing in tortuous foams likely limits the development of boundary layers typically found in honeycomb monoliths and aids the use of simplified solution treatments such as plug flow.

In view of these factors, a plug-flow model was coupled with empirical temperature profiles to simulate effluent species profiles during the lightoff of a foam monolith. Because the complex foam geometry is ignored in the straight-channel simulations, differences between gas-phase conditions and those at the gas–catalyst interface were neglected. Previous and more rigorous simulations for methane CPO on a Pt monolith showed that the gas and solid phases are thermally equilibrated within the first millimeter.[15] Empirical temperature profiles were used in lieu of a 1-D transient energy balance because of the complex nature of the combustion phase. Numerical simulations in this work attempted to capture the surface chemistry occurring after the switch from total to partial oxidation stoichiometry and draw useful conclusions about catalyst temperature development during lightoff. A 1D transient energy balance applied after combustion would only be as accurate as the initial conditions for the monolith's axial temperature profile once the stoichiometry was switched. Because this profile has not been well defined experimentally or numerically through a more sophisticated physical treatment,

the presumed effect of the combustion phase on the monolith was lumped in the empirical temperature profiles.

Temperature profile parameters

The temperature parameters iteratively determined in the simulations give good agreement between experimental and numerical species profiles. However, the temperature profiles and their accompanying best-fit parameters should be additionally bounded by theory. The length chosen for the CPO oxidation section (1 mm) is an upper bound and agrees well with more rigorous simulations solving the 1D energy equation.[15] For short-time combustion experiments exhibiting no temperature overshoot (such as a 1-s combustion time experiment), heating of the catalyst back face to steady-state temperature should be dominated by two time constants: the time constant for the front-face temperature to reach steady state, and the effective diffusion time constant for the remainder of the monolith.

The first time constant can be approximated by the actual combustion time itself (such as 1 to 1.5 s). From diffusion theory, an upper bound for the second time constant can be approximated as α/δ^2, where α is the thermal diffusivity of the alumina monolith and δ is the catalyst's axial length. A typical value for the alumina monolith thermal diffusivity (including monolith porosity) is 6.7×10^{-6} m^2/s.[27] Note that this value is an upper bound, given that transport inside the porous monolith is advective and not just diffusive. Combining this value with the catalyst length (5 mm) gives a time constant of 3.7 s. These theoretical time constants can be tested by fitting experimental back-face temperature data to a second-order plus time delay fit. This approach should be reasonably robust because the thermocouple used to measure back-face temperature possesses a rapid response time ($<$0.3 s). For 1-s combustion time experiments, minimizing the least-square error between the second-order fit and back-face temperature data gives average time constants of 1.3 and 2.2 s, with a time delay of 2.2 s. The first time constant, 1.3 s, compares well with the average 1.5-s combustion time used in experiments and the 1.1-s time constant used as a simulation parameter (Table 1). The 2.2-s effective diffusion time constant is significantly less than 3.7 s from conduction theory, but this is expected because heat transport in the monolith has a significant convective component.

The approach described above is of limited value in justifying model parameters for longer combustion times where the initial flame heats the front face above the steady-state CPO temperature causing overshoot. In this case, three time constants (heating and cooling of front face and diffusion) will control the catalyst temperature profile and retrieving them accurately from a third-order fit becomes difficult. Also, the high front-face temperatures at feed switch cause the product species to respond so quickly ($\ll$1 s), that the mass spectrometer likely misses the peak response. For this reason, errors between species profiles for the 5-s combustion time simulation and experiments were not minimized using least-squares criteria but were determined visually.

Summary

The rapid startup ($<$10 s) of a short-contact-time reactor to produce steady-state syngas from methane has been demonstrated without external preheat by initially using homogeneous combustion. Analysis of the reactor products with a rapid-response mass spectrometer allowed the determination of the optimal combustion time that minimized time delay in syngas production. One-dimensional plug-flow simulations of short combustion time experiments (1- and 5-s combustion times) demonstrated that transient product profiles can be accurately reproduced using an established surface mechanism originally used to model steady-state chemistry. Combining parameters bounded by theory for the thermal catalyst history with the plug-flow model resulted in the development of a transient, axially distributed temperature profile that offers insight into how the catalyst temperature develops during lightoff. This work helps further the state of the art in fast start-up reforming technologies for demanding fuel cell–based mobile applications.

Acknowledgments

Funding was provided in part by Delphi Automotive Corporation and the National Science Foundation under Grant CTS-0211890. K. A. Williams acknowledges funding through a National Science Foundation Graduate Research Fellowship. Special thanks go to Dr. Kevin N. West for his expertise and assistance in setting up the data-acquisition system.

Literature Cited

1. Hickman DA, Schmidt LD. Production of syngas by direct catalytic oxidation of methane. *Science.* 1993;259:343-346.
2. Hickman DA, Schmidt LD. Steps in CH_4 oxidation on Pt and Rh surfaces: High-temperature reactor simulations. *AIChE Journal.* 1993; 39:1164-1177.
3. O'Connor RP, Klein EJ, Schmidt LD. High yields of synthesis gas by millisecond partial oxidation of higher hydrocarbons. *Catalysis Letters.* 2000;70:99-107.
4. Krummenacher JJ, West KN, Schmidt LD. Catalytic partial oxidation of higher hydrocarbons at millisecond contact times: Decane, hexadecane, and diesel fuel. *Journal of Catalysis.* 2003;215:332-343.
5. Schmidt LD, Klein EJ, Leclerc CA, Krummenacher JJ, West KN. Syngas in millisecond reactors: Higher alkanes and fast lightoff. *Chemical Engineering Science.* 2003;58:1037-1041.
6. Belogub AV, Talda GB. Fuel supply system constructions of gasoline/hydrogen automobiles. *International Journal of Hydrogen Energy.* 1991;16:417-421.
7. Cohn DR, Rabinovich A, Titus CH. Onboard plasmatron generation of hydrogen for extremely low emission vehicles with internal combustion engines. *International Journal of Vehicle Design.* 1996;17:550-561.
8. Jung H, Yoon WL, Lee H, Park JS, Shin JS, La H, Lee JD. Fast start-up reactor for partial oxidation of methane with electrically-heated metallic monolith catalyst. *Journal of Power Sources.* 2003; 124:76-80.
9. Schwiedernoch R, Tischer S, Correa C, Deutschmann O. Experimental and numerical study on the transient behavior of partial oxidation of methane in a catalytic monolith. *Chemical Engineering Science.* 2003; 58:633-642.
10. Leclerc CA, Redenius JM, Schmidt LD. Fast lightoff of millisecond reactors. *Catalysis Letters.* 2002;79:39-44.
11. Bodke AS, Bharadwaj SS, Schmidt LD. The effect of ceramic supports on partial oxidation of hydrocarbons over noble metal coated monoliths. *Journal of Catalysis.* 1998;179:138-149.
12. Twigg MV, Richardson JT. Theory and applications of ceramic foam catalysts. *Chemical Engineering Research and Design.* 2002;80:183-189.
13. Deutschmann O, Schmidt LD. Modeling the partial oxidation of methane in a short-contact-time reactor. *AIChE Journal.* 1998;44:2465-2477.
14. Goralski CT, O'Connor RP, Schmidt LD. Modeling homogeneous and heterogeneous chemistry in the production of syngas from methane. *Chemical Engineering Science.* 2000;55:1357-1370.

15. Veser G, Frauhammer J. Modeling steady state and ignition during catalytic methane oxidation in a monolith reactor. *Chemical Engineering Science.* 2000;55:2271-2286.
16. Kee RJ, Rupley FM, Miller JA, Coltrin ME, Grcar JF, Meeks E, Moffat HK, Lutz AE, Dixon-Lewis G, Smooke MD, Warnatz J, Evans GH, Larson RS, Mitchell RE, Petzold LR, Reynolds WC, Caracotsios M, Stewart WE, Glarborg P. PLUG: A program for the analysis of plug-flow reactors with gas-phase and surface chemistry. *CHEMKIN Collection, Release 3.5.* San Diego, CA: Reaction Design; 1999.
17. Cleland FA, Wilhelm RH. Diffusion and reaction in viscous-flow tubular reactor. *AIChE Journal.* 1956;2:489-497.
18. Raja LL, Kee RJ, Deutschmann O, Warnatz J, Schmidt LD. A critical evaluation of Navier–Stokes, boundary-layer, and plug-flow models of the flow and chemistry in a catalytic-combustion monolith. *Catalysis Today.* 2000;59:47-60.
19. Kee RJ, Rupley FM, Miller JA, Coltrin ME, JF Grcar JF, Meeks E, Moffat HK, Lutz AE, Dixon-Lewis G, Smooke MD, Warnatz J, Evans GH, Larson RS, Mitchell RE, Petzold LR, Reynolds WC, Caracotsios M, Stewart WE, Glarborg P. TRANSPORT: A software package for the evaluation of gas-phase multicomponent, transport properties. *CHEMKIN Collection, Release 3.5.* San Diego, CA: Reaction Design; 1999.
20. Klein EJ, Tummala S, Schmidt LD. Catalytic partial oxidation of methane to syngas: Staged and stratified reactors with steam addition. *Studies in Surface Science and Catalysis.* 2001;136:245-250.
21. Kee RJ, Rupley FM, Miller JA, Coltrin ME, Grcar JF, Meeks E, Moffat HK, Lutz AE, Dixon-Lewis G, Smooke MD, Warnatz J, Evans GH, Larson RS, Mitchell RE, Petzold LR, Reynolds WC, Caracotsios M, Stewart WE, Glarborg P. EQUIL: A program for computing chemical equilibria. *CHEMKIN Collection, Release 3.5.* San Diego, CA: Reaction Design; 1999.
22. Taylor JD, Allendorf MD, McDaniel AH, Rice SF. In situ diagnostics and modeling of methane catalytic partial oxidation on Pt in a stagnation-flow reactor. *Industrial & Engineering Chemistry Research.* 2003;42:6559-6566.
23. Bizzi M, Basini L, Saracco G, Specchia V. Short contact time catalytic partial oxidation of methane: Analysis of transport phenomena effects. *Chemical Engineering Journal.* 2002;90:97-106.
24. Bizzi M, Basini L, Saracco G, Specchia V. Modeling a transport phenomena limited reactivity in short contact time catalytic partial oxidation reactors. *Industrial & Engineering Chemistry Research.* 2003;42:62-71.
25. Bizzi M, Schwiedernoch R, Deutschmann O, Saracco G. Modeling the partial oxidation of methane in a fixed bed with detailed chemistry. *AIChE Journal.* 2004;50:1289-1299.
26. Hohn KL, Schmidt LD. Partial oxidation of methane to syngas at high space velocities over Rh-coated spheres. *Applied Catalysis A: General.* 2001;211:53-68.
27. Lide DR, ed. *CRC Handbook of Chemistry and Physics*. 75th ed. Boca Raton, FL: CRC Press; 1994.

Manuscript received Feb. 6, 2004, and revision received May 18, 2004.